Paper accepted for publication in Journal of Sound and Vibration, 23 May 2023:
https://doi.org/10.1016/j.jsv.2023.117818

The sound radiation from a periodic array of railway sleepers using a wavenumber domain method

Hui Li[a], Xinbiao Xiao[b], David Thompson[c], Giacomo Squicciarini[c]

[a] State Key Laboratory of Vehicle NVH and Safety Technology, Changan Auto Global R&D Center, Changan Automobile Co., Ltd., Chongqing 401120, China

[b] State Key Laboratory of Traction Power, Southwest Jiaotong University, Chengdu 610031, China

[c] Institute of Sound and Vibration Research, University of Southampton, Southampton SO17 1BJ, United Kingdom

Abstract

Rolling noise, radiated by the vibration of the wheels, and the track, is an important source of noise from railway operations. In ballasted track the sleepers supporting the rails form an important source of noise at low frequencies. There are difficulties to calculate their sound radiation using numerical models due to their discrete periodic nature and the infinite extent of the track. For the rail, which has invariant geometry in the axial direction, the wavenumber domain (2.5D) finite element or boundary element method can be used to calculate the vibration and noise radiation. However, the 2.5D method cannot be used directly to predict the vibration and sound radiation of railway sleepers due to their discrete spacing. In this work, the discrete spacing of the sleepers in the spatial domain is introduced into the 2.5D method by applying a series of rectangular windows according to the sleeper width and spacing. The vibration of the sleepers in the wavenumber domain is obtained by applying a spatial Fourier transform to the product of these windows and the rail transfer mobility, also allowing for the ratio between the sleeper vibration and the rail vibration. The sleeper radiation obtained from the proposed approach is compared with the result obtained from the Rayleigh integral method, showing good agreement. The mobilities of the sleepers in the wavenumber domain are used to explain the effect of the sleeper spacing on the sound radiation. The spectrum of response in the wavenumber domain contains multiple waves, shifted in wavenumber by multiples of $2\pi/L$, where L is the sleeper spacing. At low frequency, only the fundamental wave corresponding to the rail wavenumber radiates power to the far field; the ratio of the sound power of discrete sleepers to that of continuous sleepers is shown to be equal to the square of the width-to-spacing ratio. As the frequency increases,

new wave branches enter the acoustic wavenumber range, leading to peaks in the radiation efficiency. At high frequency, the ratio of the sound powers converges to a constant value equal to the ratio of areas.
Key words: wavenumber, 2.5D, boundary element method, sleeper radiation, railway track, windows.

1 Introduction

Railway noise can be a source of annoyance to lineside residents and an important factor affecting passenger comfort inside trains. In many situations, and over a wide speed range, the most important source of noise from railway operations is rolling noise [1]. The rolling noise is radiated by the vibration of the wheels and track, induced by their combined surface roughness; both the wheels and the track radiate significant proportions of the noise.

Prediction models for rolling noise were first developed by Remington [2, 3], who used analytical models for the sound radiation. The TWINS model [4, 5] was developed as an extension of the same framework, making use of numerical models for some aspects, for example using finite element (FE) modelling for the wheel and rail vibration [6, 7]. To determine the radiation of sound from the wheel vibration, axisymmetric boundary elements (BE) were used and the results expressed as radiation efficiencies for wheel modes with different numbers of nodal diameters [8]. Simplified formulae were then derived to approximate the BE results. Axisymmetric BE solutions for the radiation from a rotating wheel have been presented more recently in [9], and in [10] the effect of a rigid ground beneath the wheel was considered.

For the rail radiation, two-dimensional (2D) BE models have been used [1] which capture the main features of the radiation at frequencies where wave propagation occurs in the rail. It was shown in [11] that the 2D BE models give satisfactory results above 250 Hz for most practical parameters of railway tracks. In [12] a 2D BE approach was used to study the influence of the proximity of the ground on the rail radiation. To take account of the waves propagating in the rail, a 2.5D FE/BE approach has been used by several authors [13-16]. The

noise from the concrete slab of a slab track has also been predicted using 2.5D methods [15-18].

The 2.5D approach is based on the assumption that the geometry and other properties are invariant along the third direction. The responses are expressed in the wavenumber domain by applying a Fourier transform to the 3D responses with respect to this third direction. This can reduce the original problem to a series of 2D ones. After the wavenumber domain solutions are obtained, an inverse Fourier transform is applied to convert the solutions back to the spatial domain. The benefits of using a 2.5D method are manifold. Only the cross-sections of the structures in one of their 2D planes are meshed, which reduces the computational effort and means that the numerical models are easier to create and amend, while retaining a similar accuracy to the corresponding 3D models. For these reasons, 2.5D methods have been used in many applications. One of the first examples of the 2.5D BE method used in acoustics was made by Duhamel [19] to predict the sound pressure around a noise barrier with constant properties in one direction but with arbitrary cross-section. The method showed high efficiency and accuracy for such a problem.

Although 2.5D methods have been used for rail vibration and radiation, in practice rails are discretely supported, and consequently there are different acoustic boundary conditions at the sleepers and between them. At the sleepers, the bottom of the rail foot is in contact with the rail pad and is unable to radiate sound, whereas between the sleepers there is a gap beneath the rail foot. This effect was considered empirically by Zhang et al. [20] who used a combination of 2D models for the two regions. Comparisons were made with a 3D BE model, from which it was shown that the sound powers of these two regions should be combined according to the ratio of their lengths for frequencies at which the acoustic wavelength is greater than the sleeper spacing, but at lower frequencies the square of this ratio should be used. Although this gave good agreement with the 3D model, the reason for this effect was not explained.

In ballasted track the sleepers are also an important source of noise. At low frequencies they have a similar vibration level to the rail but, due to their larger area, they have a larger radiation efficiency and produce a greater sound power. In the TWINS model the radiation efficiency of the sleepers was estimated using a simple model of a baffled piston, representing the upper surface of the sleeper, with some corrections applied for the

interaction of multiple sleepers [21]. In [22] a BE model of a single sleeper was used as part of an optimization procedure. The bottom of the sleeper was fixed on a rigid plane and the model was used to determine the radiation efficiency.

Zhang et al. [23] used a Rayleigh integral method to estimate the radiation efficiency of single or multiple sleepers excited by a rail. It was shown that it is normally sufficient to include three sleepers in determining the radiation efficiency. At low frequencies, due to the high decay rate in the rail, only three sleepers are excited by a force on the rail, the vibration of sleepers further from the force being negligible. At higher frequencies, where the distance between them exceeds the acoustic wavelength, the sleepers radiate independently and there is no need to include larger numbers of sources in determining the radiation efficiency. The radiation efficiency of multiple sleepers was shown to exhibit peaks at frequencies at which the acoustic wavelength matched the sleeper spacing.

Li et al. [24] used a 2.5D BE model to predict the sound pressure distribution on the external surfaces of a train. The wheels were represented as point sources whereas the rails were modelled using their cross-section with the vibration obtained from a Timoshenko beam model. The radiation from the sleepers was also modelled using a 2.5D BE model, with the effect of the discrete spacing represented by a scaling factor derived from a Rayleigh integral model, similar to the approach used in [23].

In the present paper the sound radiation from a periodic array of discretely spaced sources, representing the sleepers, is modelled using the 2.5D BE approach. To introduce the discrete spacing, a window function is applied to the wavenumber spectrum, as proposed by Theyssen [25]. From analysis of the wavenumber spectra with and without this window function, the weighting functions used by Zhang et al. [23] and Li et al. [24] are explained theoretically. The rest of the paper is organised as follows: the 2.5D BE method is briefly introduced in Section 2. The modelling of the vibration of discrete sleepers in the 2.5D domain is described in Section 3. In Section 4, comparisons are presented of the sleeper radiation obtained using the current approach and the Rayleigh integral method. Section 5 investigates the effect of sleeper spacing on its sound radiation. Conclusions are drawn in Section 6.

2 Wavenumber domain BE method

To be able to apply the 2.5D BE method, it is assumed that the geometry of the problem can be considered invariant and of infinite length in one direction, here denoted x. The following Fourier transform pair for the sound pressure $p(x, y, z)$ with respect to *x* can be introduced

$$\tilde{p}(k_x, y, z) = \int_{-\infty}^{\infty} p(x, y, z)\, \mathrm{e}^{\mathrm{i}k_x x} \mathrm{d}x \tag{1}$$

$$p(x, y, z) = \frac{1}{2\pi} \int_{-\infty}^{\infty} \tilde{p}(k_x, y, z)\, \mathrm{e}^{-\mathrm{i}k_x x} \mathrm{d}k_x \tag{2}$$

where k_x is the wavenumber in the x direction, i is the imaginary unit and time-harmonic variations are assumed with dependence $\mathrm{e}^{\mathrm{i}\omega t}$ (ω is the angular frequency). The spatial distribution of sound pressure can then be obtained from Eq. (2) once $\tilde{p}(k_x, y, z)$ has been determined. This can be achieved through a 2.5D formulation of the boundary integral equation in which the pressure, velocity and Green's functions are expressed in terms of k_x, y and z, and the boundary integrals are solved over the perimeter of the boundary region Γ in the *y*-*z* plane. This is effectively a 2D BE problem for each combination of ω and k_x.

The sound power, W, radiated by the infinitely long vibrating surface can be written as [14]

$$W = \frac{1}{2} \mathrm{Re} \left(\int_{-k_0}^{k_0} \int_{\Gamma} \tilde{p}^*(k_x) \tilde{v}_n(k_x)\, \mathrm{d}\Gamma \mathrm{d}k_x \right) \tag{3}$$

where Γ is the perimeter of the cross-section of the vibrating structure in the *y*-*z* plane, $k_0 = \omega/c_0$ is the wavenumber in air, with c_0 the speed of sound in air. $\tilde{v}_n$ is the normal velocity and $\tilde{p}$ is the sound pressure on their cross-section, and the symbol * indicates the complex conjugate. In Eq. (3), the integral over k_x is limited to the range $\pm k_0$ since, for larger values of k_x, no power is radiated to the far field. The power can be normalised to give the radiation efficiency, which can be written as

$$\sigma = \frac{W}{\frac{1}{2} \rho_0 c_0 \int_{-\infty}^{\infty} \int_{\Gamma} |\tilde{v}_n(k_x)|^2\, \mathrm{d}\Gamma \mathrm{d}k_x} \tag{4}$$

where ρ_0 is the density of air.

3 Sleeper vibration in wavenumber domain

3.1 Rail vibration

In a typical ballasted track, the rails are supported by rubber rail pads on sleepers, usually made of concrete, which are in turn laid in ballast. Various models have been developed for the track vibration [1]. In the current work the rail is represented by an infinite Timoshenko beam on supports consisting of equivalent continuous layers of damped springs for the rail pads, masses for the sleepers and further damped springs for the ballast, as shown in Figure 1. The mass and stiffness per unit length are obtained by dividing the values per sleeper by the sleeper spacing [1]. Damping is included by introducing complex stiffnesses of the form $K(1+\mathrm{i}\eta)$, where K is the corresponding stiffness and η is the loss factor; similarly damping is added to the rail by making the Young's modulus and shear modulus complex using a loss factor. In more advanced models the discrete nature of the supports and the cross-section deformation of the rail can be included [26]; the sleepers can also be represented by flexible beams [27]. The current approach for the sound radiation of the sleepers could be applied to each of these, but the simple continuously supported beam model is used here for simplicity.

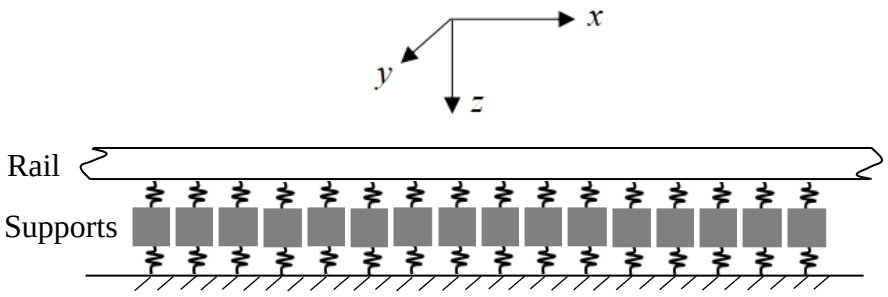

Figure 1. A sketch of a continuously supported railway track with coordinate system.

If a point force is applied to the rail at x = 0, its response consists of a propagating wave and an evanescent wave on each side of the excitation point. The response of the rail at frequency ω (assuming a time dependence of $\mathrm{e}^{\mathrm{i}\omega t}$) can be written in the form of a transfer mobility from a unit force at x = 0 to the velocity response at a distance x [1]

$$Y(x) = u_1 \mathrm{e}^{-\mathrm{i}k_r|x|} - \mathrm{i}u_2 \mathrm{e}^{-\beta|x|} \tag{5}$$

where k_r is the structural wavenumber corresponding to the predominantly propagating wave, β is the one corresponding to the evanescent wave and u_1 and u_2 are the associated wave

amplitudes. By solving the appropriate equations of motion these wavenumbers and amplitudes can be obtained, including the effect of the support layers [1]. The velocity response can be expressed in the wavenumber domain by applying a Fourier transform, similar to Eq. (1). This yields [24]

$$\tilde{Y}(k_x) = u_1\left(\frac{1}{\mathrm{i}(k_r + k_x)} + \frac{1}{\mathrm{i}(k_r - k_x)}\right) - \mathrm{i}u_2\left(\frac{1}{\beta + \mathrm{i}k_x} + \frac{1}{\beta - \mathrm{i}k_x}\right) \tag{6}$$

where k_x can take values from $-\infty$ to ∞.

Table 1 lists the properties of a typical track fitted with a UIC 60 rail and soft rail pads, which are used for the simulations here. Based on these properties, the propagating wavenumber k_r of the rail for the vertical direction is shown in Figure 2. The vertical transfer mobility of the rail is calculated from Eq. (5) as a function of frequency and presented in Figure 3 for three values of x: x = 0 (the driving point), x = 0.6 m (the nominal sleeper spacing) and x = 1.2 m. Two obvious peaks below 1 kHz can be seen in Figure 3 in the vertical mobility. The first occurs at around 180 Hz, which is the resonance of the combined mass of the rail and sleeper on the vertical ballast stiffness. The second peak, at about 370 Hz is the vertical resonance of the mass of the rail on the stiffness of the rail pad [1]. After the second peak, waves cut on in the rail (the imaginary part of the wavenumber becomes small) and the magnitude of the mobility does not decrease significantly with distance.

Table 1. Parameters used to represent vertical vibration of a railway track.

Parameter	Value
Rail bending stiffness (Nm^2)	6.42×10^6
Rail shear coefficient	0.4
Rail loss factor	0.02
Mass per length (kg/m)	60
Pad stiffness per unit length (N/m^2)	1.83×10^8
Pad loss factor	0.2
Half sleeper mass per unit length (kg/m)	233
Sleeper width (m)	0.2
Ballast stiffness per unit length (N/m^2)	3.33×10^8
Ballast loss factor	1.0

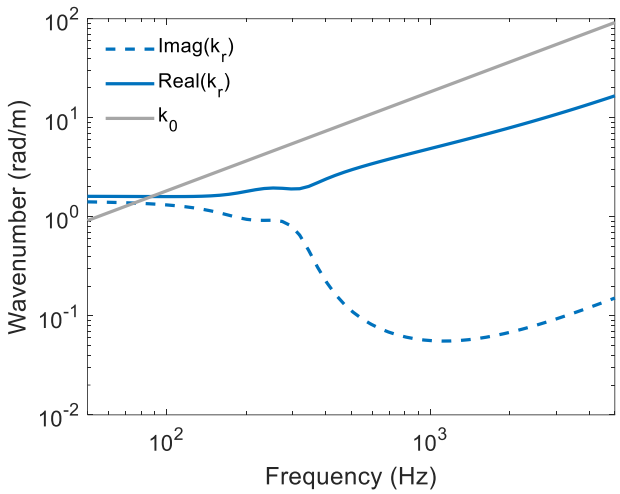

Figure 2. The propagating wavenumber k_r of the rail for the vertical direction as a function of frequency. k_0 is the acoustic wavenumber.

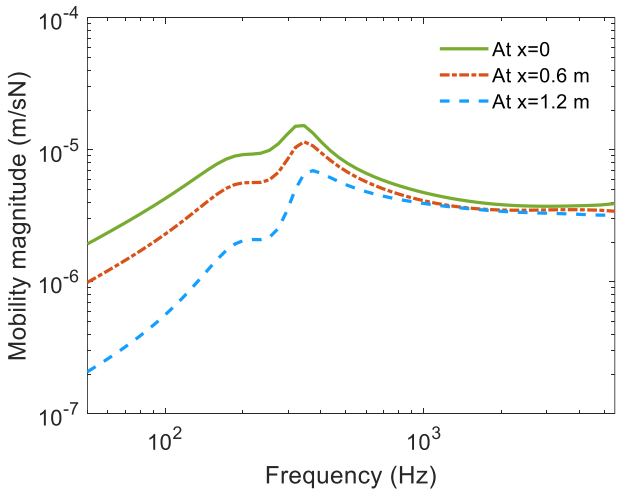

Figure 3. Rail point and transfer mobilities for the vertical direction as a function of frequency.

The transfer mobility of the rail is plotted in Figure 4 as a function of distance for two example frequencies, 125 Hz and 630 Hz. This illustrates the high decay rate at 125 Hz, whereas at 630 Hz the waves propagate with a much lower decay rate. The corresponding mobilities in the wavenumber domain are shown in Figure 5 (similar results were shown for different parameters in [24]; more complete 3D plots are given by Theyssen [25]). At high enough frequency, once propagating waves have cut on in the rail, the wavenumber spectrum is dominated by the free wavenumber in the rail; at 630 Hz this can be seen as the peak at about 3.6 rad/m.

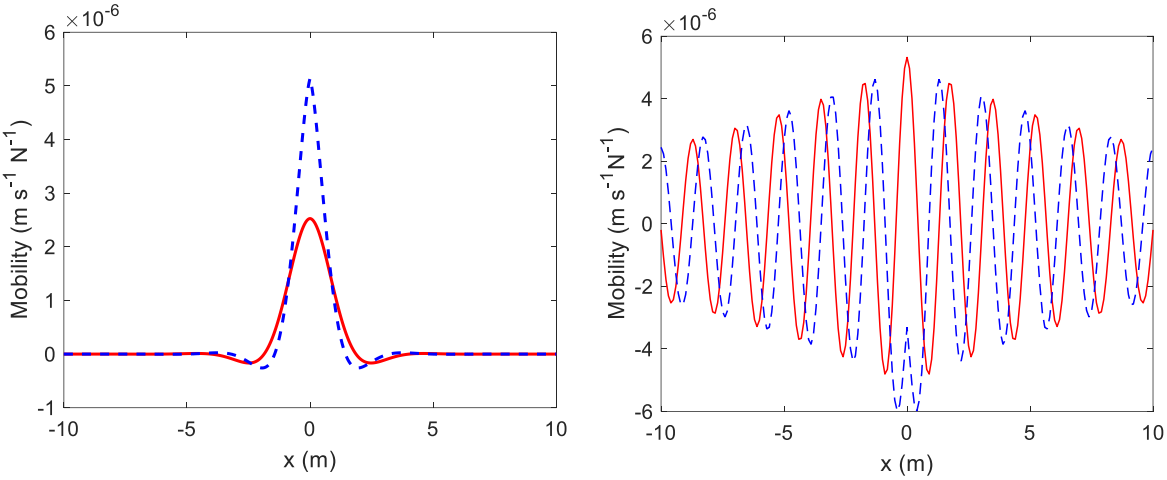

(a) (b)

Figure 4. Rail transfer mobility for the vertical direction as a function of x, ——: real part; – – –: imaginary part. (a) 125 Hz, (b) 630 Hz.

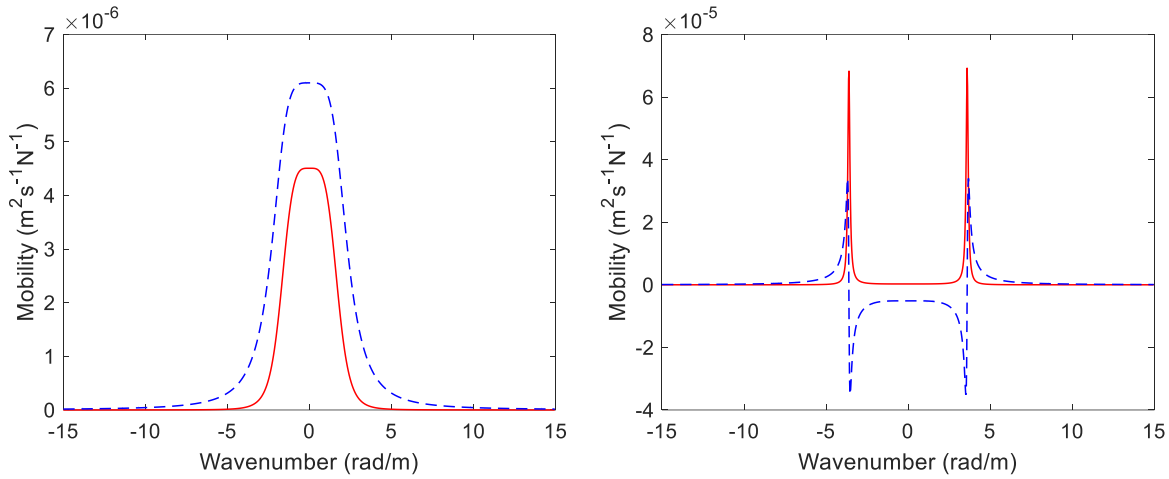

(a) (b)

Figure 5. Rail mobility in the wavenumber domain, ——: real part; – – –: imaginary part. (a) 125 Hz, (b) 630 Hz.

3.2 Sleeper vibration

For the model in Figure 1, the vibration of the sleepers at a position x can be determined from the vertical rail vibration at that position. The ratio of the sleeper velocity to that of the rail is given by [1]

$$\tau(\omega) = \frac{K_p}{K_p + K_b - \omega^2 m_s} \tag{7}$$

where K_p is the complex rail pad stiffness in the vertical direction including damping, K_b is the complex ballast stiffness and m_s is the mass of half a sleeper. The same equation can be

used when the values are expressed per unit length as in Table 1. This ratio is plotted against frequency in Figure 6 for the current parameters. This has a peak at about 250 Hz, which lies between the two peaks identified in the rail mobility. At this frequency the sleeper mass vibrates between the two layers of springs and acts like a dynamic absorber to the rail, increasing its decay rate. Above this frequency the magnitude of the sleeper vibration reduces rapidly with increasing frequency.

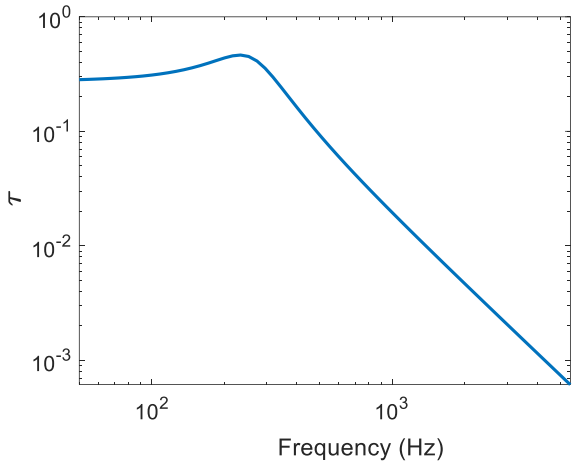

Figure 6. The ratio of the sleeper velocity to that of the rail.

Although this model of the track vibration represents the sleepers as a continuous layer, the response of discrete sleepers can be approximated by extracting the vibration at the positions of the sleepers. Alternatively, assuming that the rail vibration does not vary significantly within the width of a sleeper, a series of rectangular windows can be applied, defined according to the sleeper width and sleeper spacing. The idea of combining spatial windows with the wavenumber domain method was presented for a finite length panel by Kim et al. [28] and more recently was introduced for the current problem of periodic sleepers by Theyssen [25]. If the force at $x = 0$ is applied directly above a sleeper, the window function is expressed as

$$w(x) = \begin{cases} 1, & x \in [-a \pm nL, a \pm nL]; \quad n = 0,1,2,\ldots \\ 0, & \text{elsewhere} \end{cases} \tag{8}$$

where a is half the sleeper width and L is the sleeper spacing, as indicated in Figure 7.

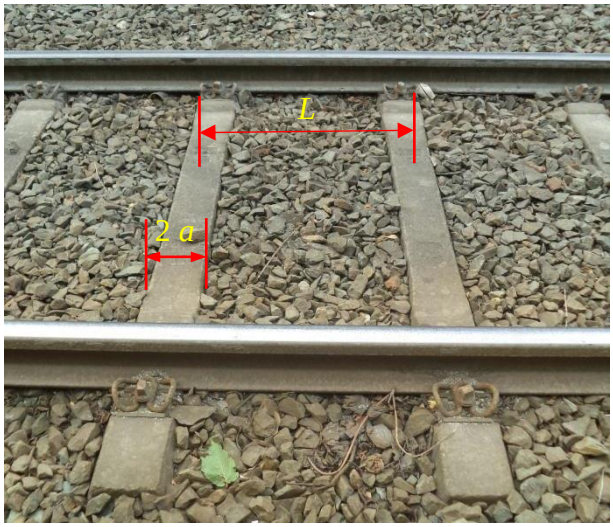

(a)

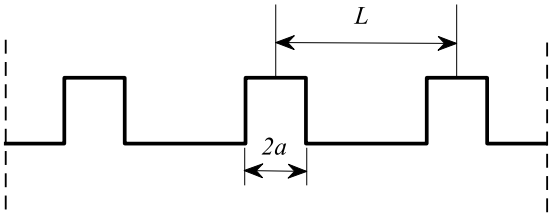

(b)

Figure 7. (a) A typical railway track, (b) rectangular windows connected in series to represent the discrete sleepers. a is a half of the sleeper width and L is the sleeper spacing.

Applying a Fourier series to the rectangular windows, Eq. (8) becomes [29]

$$w(x) = a_0 + \sum_{n=1}^{\infty} a_n \cos\left(\frac{2n\pi}{L}x\right) + b_n \sin\left(\frac{2n\pi}{L}x\right) \tag{9}$$

where the coefficients a_0, a_n, b_n are calculated as

$$a_0 = \frac{2a}{L}, \quad a_n = \frac{2}{n\pi}\sin\left(\frac{2n\pi}{L}a\right), \quad b_n = 0 \tag{10}$$

The transfer mobility of the sleepers in the spatial domain (for a unit force on the rail at x = 0) is equal to the transfer mobility of the rail multiplied by the vibration ratio $\tau(\omega)$ (Eq. (7)) and then multiplied by the rectangular windows $w(x)$ (Eq. (9)). Applying a Fourier transform to this, the velocity of the sleepers in the wavenumber domain due to a unit force at x = 0 is obtained as

$$\widetilde{Y}_s(k_x) = \tau(\omega) \int_{-\infty}^{+\infty} Y(x) w(x) \mathrm{e}^{\mathrm{i}k_x x} \, \mathrm{d}x$$
$$= \tau(\omega) \sum_{n=0}^{\infty} a_n \frac{\tilde{Y}\left(k_x + \frac{2n\pi}{L}\right) + \tilde{Y}\left(k_x - \frac{2n\pi}{L}\right)}{2} \tag{11}$$

where $\tilde{Y}(k_x)$ is the mobility of the rail in the wavenumber domain. After applying these windows, the mobility of the sleepers is given by a sum of terms which contain the mobility of the rail shifted in wavenumber by $\pm 2n\pi/L$. The fact that the wavenumbers occur with a repeating pattern with a shift of $\pm 2\pi/L$ has been noted previously e.g. in Ref. [30] for a slab track with periodic supports and in Ref. [25] for the vibration of periodic sleepers. These terms in Eq. (11) are weighted by different coefficients $a_n/2$. The mobility of the sleepers in the wavenumber domain at two frequencies, 125 Hz and 630 Hz, is shown in Figure 8, based on the parameters in Table 1 and a nominal spacing of 0.6 m. Compared with the rail mobility in Figure 5, additional peaks can be seen that are introduced by the terms in the series. For the sleeper spacing of 0.6 m used here, these are shifted by multiples of 10.5 rad/m.

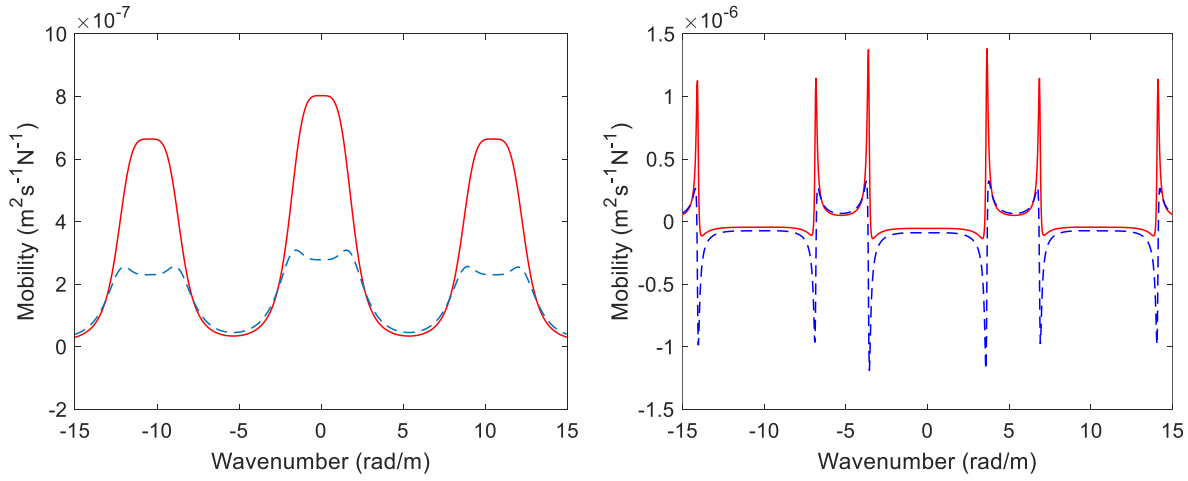

(a) (b)

Figure 8. Sleeper mobilities in the wavenumber domain, ——: real part; - - -: imaginary part. (a) 125 Hz, (b) 630 Hz.

4. 2.5D approach for sleeper radiation

4.1 Implementation of the 2.5D BE method for the sleepers

To calculate the sound radiation from the sleepers using the 2.5D BE model, a 2D mesh of the sleeper cross-section is required. As the sleepers are buried in the ballast, and they are

mainly vibrating in the vertical direction, it is assumed that only the top surfaces will radiate sound. The absorption of the ballast is neglected. In this work, the sleepers are represented by a rectangular box with a height of 0.05 m located on a rigid ground, i.e. using a halfspace model, as shown in Figure 9. In the present work the bending vibration of the sleepers is neglected. For simplicity, half the sleeper length (1.25 m) is included in the model and the sleeper vibration is assumed to be uniform over its whole upper surface. Linear boundary elements with a length 0.01 m are used to create the mesh, which gives at least six elements per wavelength up to 5 kHz, and five 'CHIEF' points are used [31] which are evenly distributed within the sleeper.

In the 2.5D formulation, the frequency ω is fixed and the results are obtained at a spectrum of wavenumbers k_x for each frequency. Consequently, results are required at M frequencies and at each frequency for N wavenumbers k_x. In this work the results are calculated at 63 frequency points in the range (46, 5620) Hz with logarithmic spacing so that there are at least three frequencies in each one-third octave frequency band. When calculating the radiated sound power using Eq.(3), the resolved wavenumber range at each frequency is (0, k_0) because the waves with wavenumbers greater than k_0 will not radiate sound power into the far field. The results for the negative wavenumbers are constructed based on those with positive wavenumbers using symmetry. A wavenumber spacing $\Delta k = 2\pi/c$ is used after verifying that this gives consistent results. When calculating the radiation efficiency using Eq.(4), a sufficiently wide range of wavenumbers is resolved at each frequency to give a good approximation to the infinite integral in the denominator. To this end, in Eq. (4), the integral over k_x in the denominator is extended to cover the range $\pm 2\pi \times 5620/c$ for all the resolved frequencies.

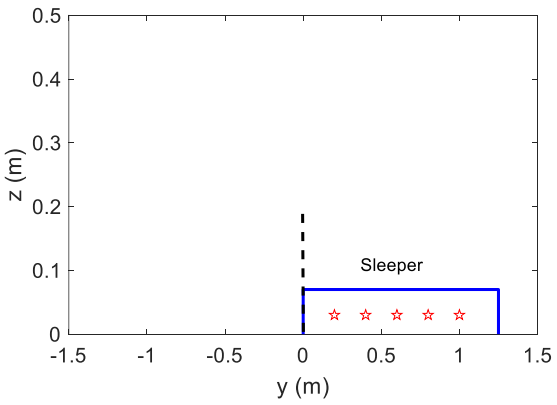

Figure 9. Sleeper model in the 2.5D domain, the stars represent the 'CHIEF' points.

4.2 Validation of the approach for sleeper radiation

For comparison, the Rayleigh integral [32] is used to calculate the sound power radiated from the discrete sleepers. For this, all the sleepers in a region 60 m long on each side of the excitation point are considered. Each sleeper has a radiating surface of 1.25×0.2 m which is assumed to be flush with the rigid ground. The sleepers are subdivided into small square segments with size 0.01×0.01 m (smaller sizes were tried but this did not affect the results). To allow a direct comparison with the 2.5D results, the vibration of the sleepers is determined in the spatial domain using $Y(x)w(x)\tau$, where $Y(x)$ is the spatial response of the rail at x, $w(x)$ is the rectangular window series (Eq. (9)) and τ is ratio of the sleeper displacement to that of the rail (Eq. (8)). This introduces a small variation with x within each sleeper that is not present in practice, where instead a constant value will apply over the whole width of the sleeper.

The sound power and radiation efficiency of the sleepers obtained by using the 2.5D BE method proposed in this paper and the Rayleigh integral method are compared in Figure 10. The track vibration is calculated using the parameters in Table 1 and a sleeper spacing of 0.6 m is used. The results from the two methods are very similar with differences of less than 0.5 dB at the peaks and less than 0.2 dB at the plateau above 2 kHz.

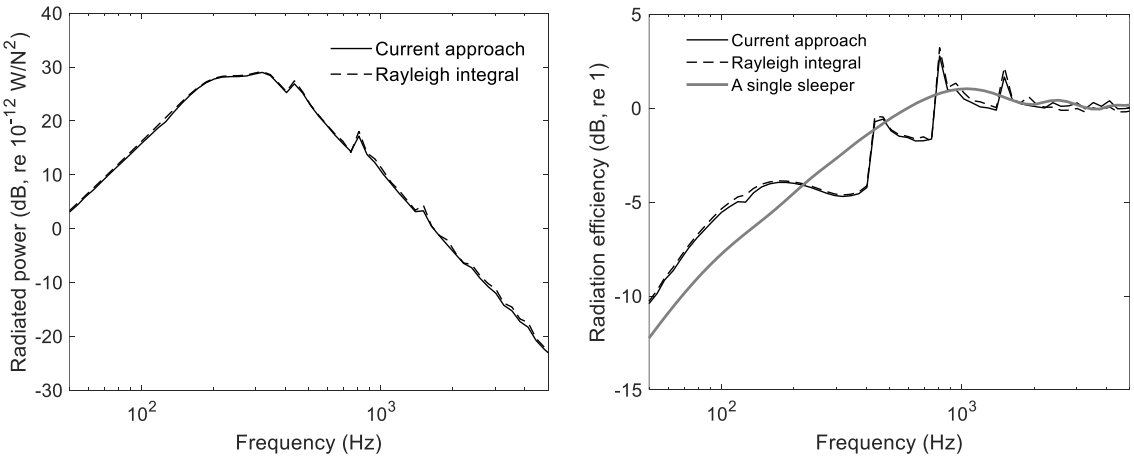

(a) (b)

Figure 10. Sound power and radiation efficiency of the sleepers obtained from different models. (a) Sound power for unit force on the rail, (b) radiation efficiency.

For comparison, the radiation efficiency of a single sleeper with uniform motion is also shown in Figure 10(b), calculated using the Rayleigh integral method. Compared with the result for the single sleeper, the radiation efficiency is increased by up to 2 dB at low

frequencies due to the influence of adjacent sleepers [23]. A few peaks appear in the sound power and radiation efficiency of the sleepers at higher frequencies. The first is at about 435 Hz, the second is around 810 Hz, and the third is at about 1505 Hz. Apart from the three main peaks, there are other small peaks which are less obvious. These will be discussed further below.

5 Effect of sleeper spacing on its radiation

5.1 Results for different sleeper spacing

To investigate the effect of the sleeper spacing on the sound power from the sleepers, four different values of sleeper spacing are considered. In each case the vibration is calculated using the parameters given in Table 1, i.e. the same values of support stiffness and sleeper mass per unit length are used. The sleepers have a width $2a$ of 0.2 m in each case. The original sleeper spacing is 0.6 m, which gives a spacing-to-width ratio $L/2a$ of 3. Three other values, 0.2 m, 0.4 m, and 1.0 m are also considered. The spacing of 1.0 m forms a wider gap between sleepers and is used on some metro and light rail systems. In this case $L/2a = 5$. The spacing of 0.4 m, with $L/2a = 2$, is not realistic but it helps to confirm the trends. These values of $L/2a$ are listed in Table 2 together with corresponding factors in decibels that will be discussed below. When the sleeper spacing is set to 0.2 m, equal to the sleeper width, it becomes equivalent to a continuously supported track. To some extent this resembles a slab track, although the effect of the bending stiffness of the slab is neglected and the mass and support stiffness will also be significantly different for a slab track. The sound radiation from a slab track is considered in detail in Ref. [17], which shows that the radiation ratio is close to unity above 60 Hz.

Table 2. Sleeper spacing-to-width ratio and corresponding factors in sound power level

Sleeper spacing	$L/2a$	$10\log_{10}(2a/L)^2$	$10\log_{10}(2a/L)$
1.0 m	5	–14.0 dB	–7.0 dB
0.6 m	3	–9.5 dB	–4.8 dB
0.4 m	2	–6.0 dB	–3.0 dB

Figure 11(a) shows the sound power radiated by the sleepers with different spacings calculated using the current method. The sleepers with wider gaps radiate less sound as their radiating surfaces are reduced. In addition, their radiation efficiency is reduced. Figure 11(b)

plots the differences between the sound power levels (SWL) for the various cases; this is given by the sound power level due to the discrete sleepers minus that of the continuous sleepers. For the sleepers with spacing of 1.0 m, the level difference is about –14 dB below around 200 Hz. This corresponds to a ratio of powers of $(2a/L)^2 = 1/25$, see Table 2. Above this frequency, the sound power level increases and fluctuations appear. An average difference of about –7 dB is found above 1 kHz, corresponding to the ratio of surface areas, $2a/L = 1/5$. For the sleepers with spacing 0.6 m, the level difference is about –9.5 dB below around 435 Hz and tends to an average difference of about –4.5 dB above 1 kHz. For the sleepers with spacing 0.4 m, the difference is about –6 dB below around 690 Hz and tends to an average of –2.9 dB above 1 kHz. In each case the low frequency value corresponds to a ratio of powers of $(2a/L)^2$ and the high frequency average corresponds to a ratio of $2a/L$, see Table 2.

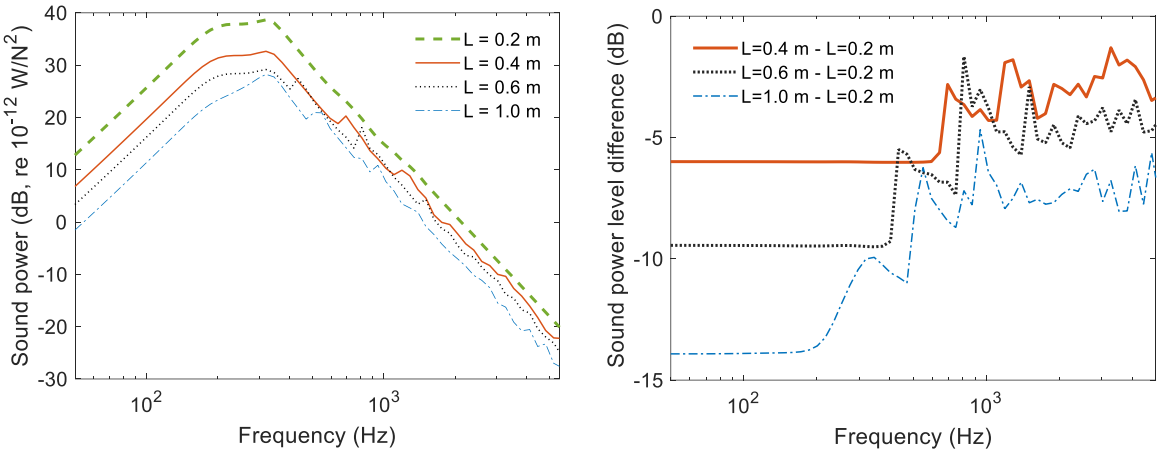

(a) (b)

Figure 11. (a) Radiated sound power of the sleepers with different spacings. (b) Sound power level difference between a track with continuous sleepers and discrete sleepers.

Zhang et al. [23] used scaling factors to convert the sound power of a continuous sleeper model into an estimate of the sound power from discrete sleepers. These were derived empirically from calculations using multiple sleepers with their vibration in a fixed amplitude ratio but with no phase difference. The scaling factors were found to be equal to the square of the width-to-spacing ratio, $(2a/L)^2$, below the frequencies at which the acoustic wavelength equals the sleeper spacing (for the three sleeper spacings considered here these frequencies are 343 Hz, 570 Hz, 857 Hz). Above these frequencies the scaling factor was found to be equal to $2a/L$ instead of its square. As discussed above, the asymptotes at low and high frequencies in Figure 11(b) agree with these scaling factors. However, the frequencies of the

first peaks in Figure 11(b) occur at about 319 Hz, 435 Hz and 693 Hz for sleeper spacings L = 1.0 m, 0.6 m and 0.4 m. These frequencies are lower than the ones estimated by Zhang et al. [23].

5.2 Interpretation of peaks in sound power spectra

To explain the occurrence of the peaks in the sleeper sound power spectra, Figure 12 shows the propagating wavenumbers in the sleeper response for a spacing of 0.6 m; these are compared with the acoustic wavenumber k_0. Only waves with wavenumbers less than the acoustic wavenumber will radiate power into the far field; these are termed supersonic waves, whereas those with wavenumber larger than the acoustic waves are subsonic and do not radiate power into the far field. The propagating wavenumber of the rail is $k_r(\omega)$, which is always supersonic, at least in the region above 370 Hz where propagating waves cut on in the rail (see Figure 2). As seen in Section 3.2, the sleeper response also contains peaks at wavenumbers $k_r \pm 2n\pi/L$. The peak at 435 Hz in the radiated power corresponds to the wave with wavenumber $-k_r + 2\pi/L$ becoming supersonic at this frequency. Similarly, the second peak at 810 Hz is due to a wave with wavenumber $+k_r + 2\pi/L$, and the third at 1505 Hz is caused by another wave with wavenumber $+k_r + 4\pi/L$. The other small peaks correspond to other new waves that appear in the supersonic region at the corresponding frequency. Similar phenomena are observed for stiffened plates by Mead [33] and for sleeper radiation by Theyssen [25].

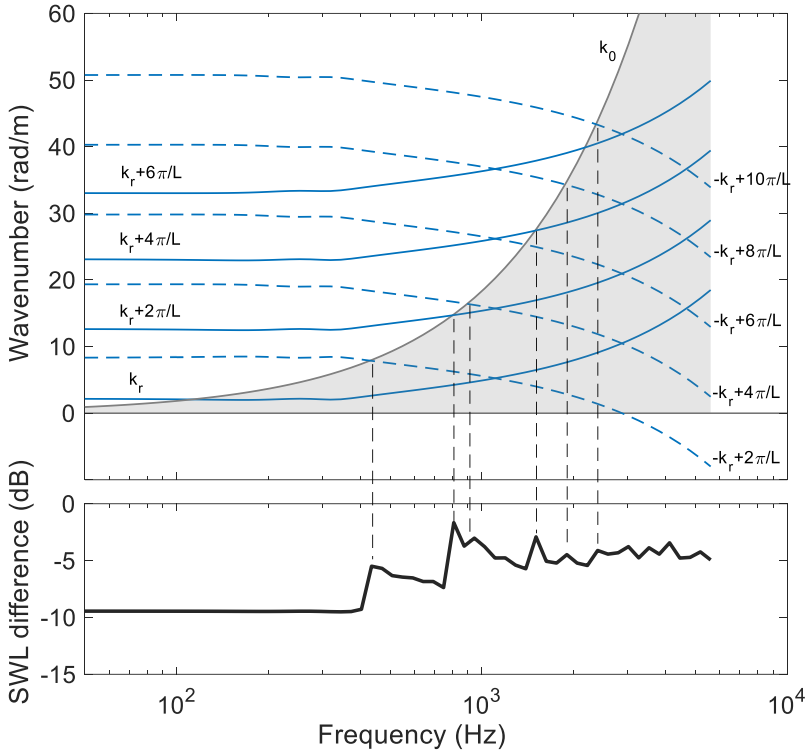

Figure 12. Top plot: propagating wavenumbers in the sleepers compared with the acoustic wavenumber (the shaded region is the supersonic region). Bottom plot: sound power level difference between discrete and continuous sleepers. In the top plot, the solid lines are the wavenumbers shifted from $+k_r$ and the dashed lines are the ones shifted from $-k_r$.

The frequencies identified by Zhang et al. [23] can be recovered using the same method by setting the rail wavenumber $k_r = 0$, so all sleepers are assumed to vibrate in phase. Then the next wavenumber would become supersonic when the acoustic wavenumber equals $2\pi/L$, or wavelength equals L, as used in [23]. However, allowing for the actual wavenumber in the rail gives better agreement with the peaks observed in the sound power.

Results are shown in Figure 13 for the discrete sleepers with spacing 0.4 m and 1.0 m. For the sleeper spacing 0.4 m, new waves enter the acoustic wavenumber range at 690 Hz and 1190 Hz in Figure 13(a). Therefore, at these two frequencies, peaks appear in the sound power. For the sleeper spacing 1.0 m, as shown in Figure 13(b), new waves enter the acoustic wavenumber range at 253 Hz, 549 Hz and 945 Hz, which causes the peaks in the sound power.

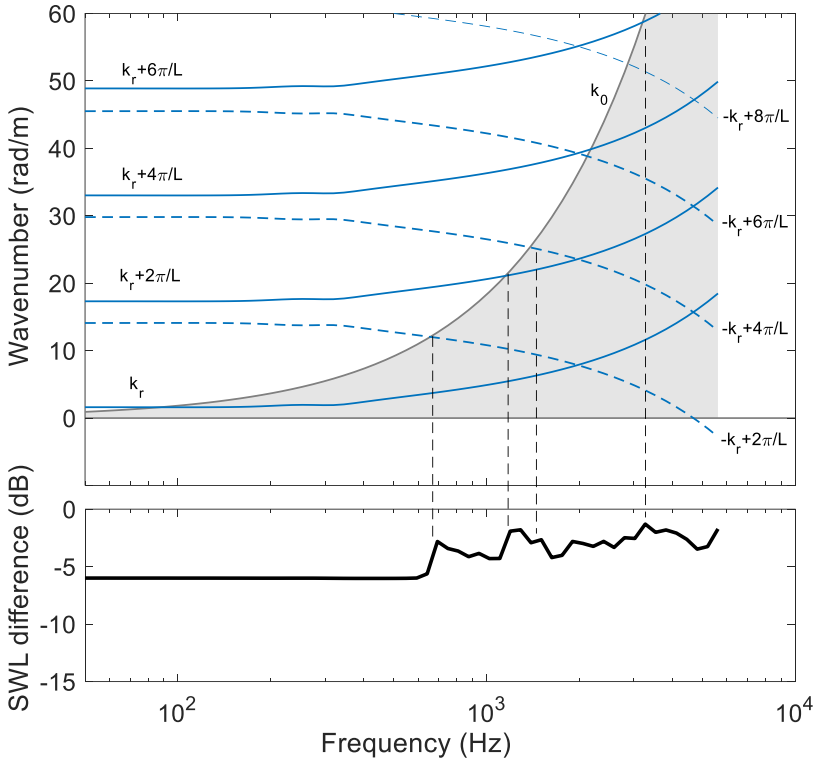

(a)

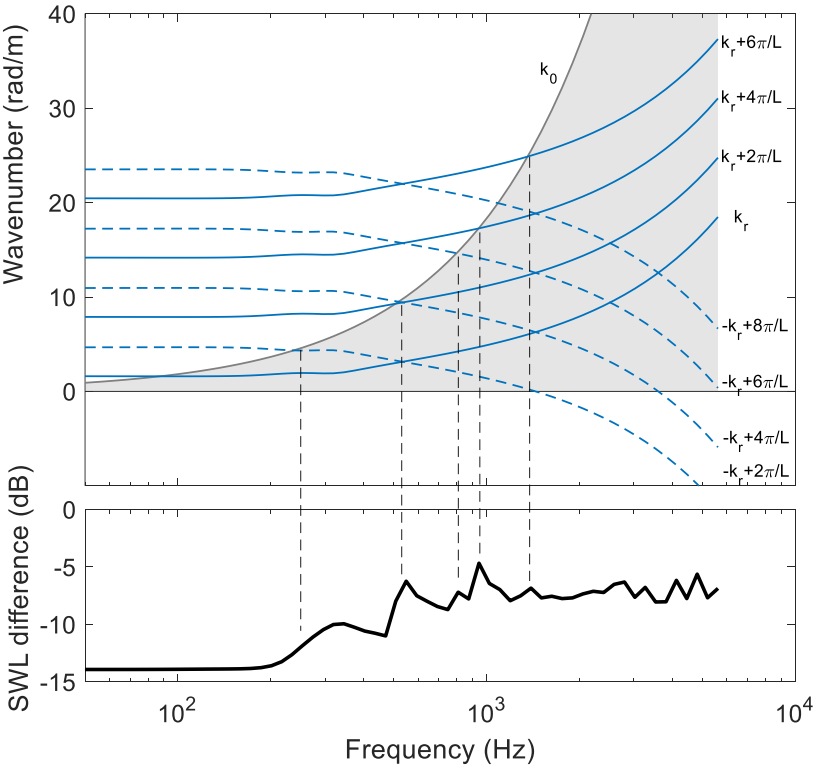

(b)

Figure 13. Top plot: propagating wavenumbers in the sleepers compared with the acoustic wavenumber (the shaded region is the supersonic region). Bottom plot: sound power level

difference between discrete and continuous sleepers. In the top plot, the solid lines are the wavenumbers shifted from $+k_r$ and the dashed lines are the ones shifted from $-k_r$. (a) L = 0.4 m, (b) L = 1.0 m.

5.3 Analysis of wavenumber spectra

To provide further quantitative explanation of the results observed in Figures 12 and 13, the vibration of the discrete sleepers in the wavenumber domain is studied. For the track with continuous sleepers, the mobility of the sleepers in the wavenumber domain can be written as $\tau\,\tilde{Y}(k_x)$ where τ is the ratio of sleeper to rail vibration and $\tilde{Y}(k_x)$ is the mobility of the rail. The mobility of the discrete sleepers is given in Eq. (11). Compared with the result for the continuous sleepers, it includes the sum of the mobilities after applying different wavenumber shifts, $\pm 2n\pi/L$, and scaling by different coefficients $a_n/2$. The magnitude of the vibration of the discrete sleepers with spacing 0.6 m is plotted in Figure 14 for two example frequencies. In these graphs the acoustic wavenumber range $(-k_0, k_0)$ is marked with the shaded region and the wavenumber shifts $\pm 2n\pi/L$ are also indicated.

At low frequency, the wavelength λ is greater than the sleeper spacing L and the acoustic wavenumber $k_0 = 2\pi/\lambda$ is smaller than the unit shift, $2\pi/L$. Consequently, only the main lobe in the mobility wavenumber spectrum is located in the range $(-k_0, k_0)$, as seen in Figure 14(a). The other lobes will not radiate sound to the far field. In such a case, only the term $a_0\tau\,\tilde{Y}(k_x)$ in Eq. (11) makes a contribution to the sound power of the discrete sleepers. Compared with the mobility $\tau\,\tilde{Y}(k_x)$ for the continuous sleepers, the one for the discrete sleepers is reduced by a factor of $a_0 = 2a/L$. The radiated power is approximately proportional to the square of the mobility. As a result, the ratio of the sound power radiated from the discrete sleepers to that of the continuous sleepers is approximately a_0^2. Therefore, at low frequency the ratio of powers is about 1/9 (–9.5 dB) for the discrete sleepers with spacing L = 0.6 m, as observed in Figure 11(b) and Table 2.

For frequencies greater than c_0/L, the acoustic wavenumber is greater than the unit shift, $2\pi/L$. Some of the side lobes in the mobility introduced by the windowing are located in the wavenumber range $(-k_0, k_0)$ and start to radiate sound to the far field. The sound radiation from the discrete sleepers increases, as observed in Figure 11. Figure 14(b) shows results at 630 Hz. The sound radiation of the continuous sleepers is dominated by free wavenumbers in the rail with peaks at $\pm$3.5 rad/m. After including the shift by $\pm 2n\pi/L$, the components with

wavenumber $(+3.5 - 2\pi/L)$ rad/m and $(-3.5 + 2\pi/L)$ rad/m enter the acoustic wavenumber range and will radiate sound to the far field.

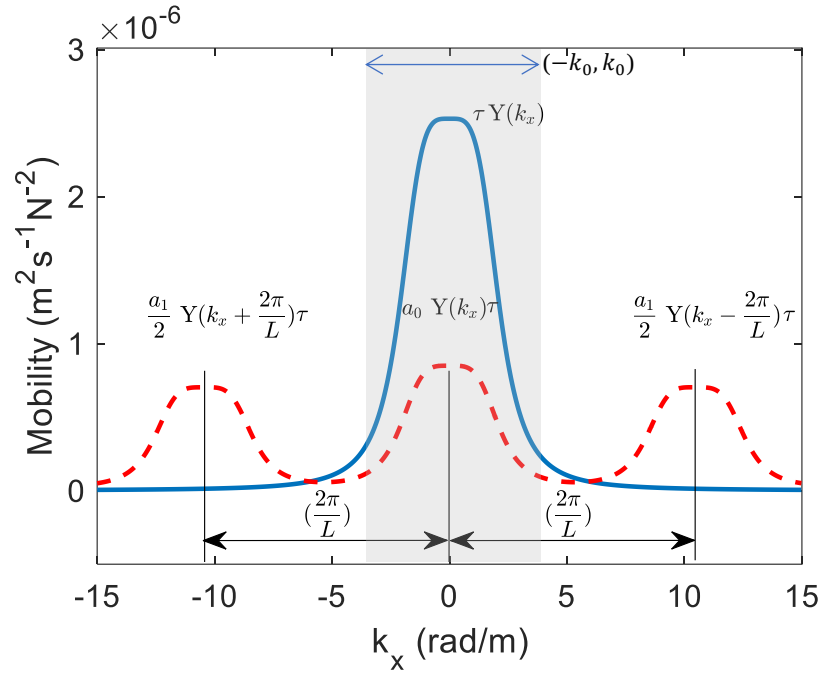

(a)

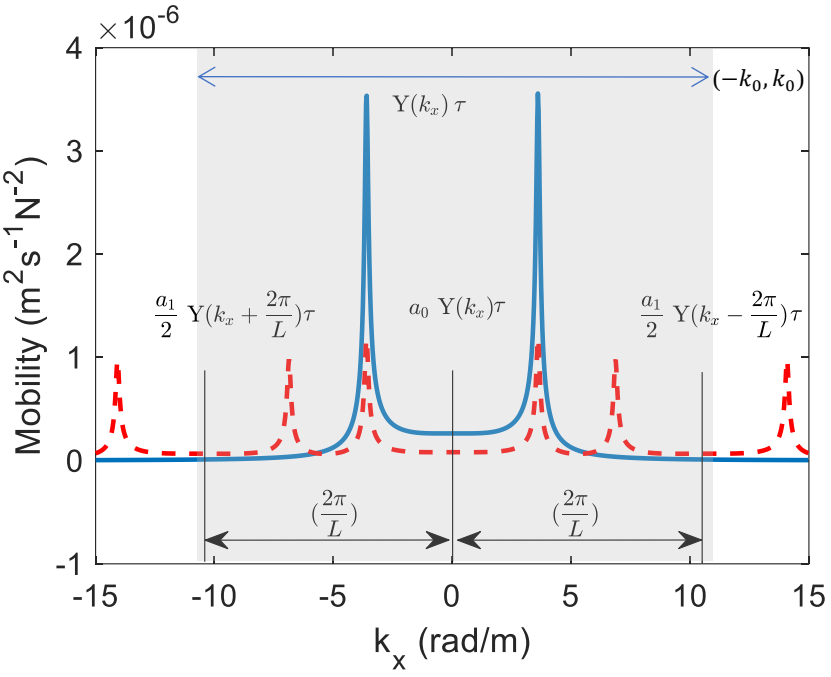

(b)

Figure 14. Mobility magnitude in the wavenumber domain. (a) 125 Hz, (b) 630 Hz. - - -: discrete sleepers with spacing L = 0.6 m, ——: continuous sleepers.

Further examples are shown in Figure 15 for two frequencies, 810 Hz and 1505 Hz, which correspond to peaks in the radiation efficiency in Figure 11(b). At each of these frequencies, a new peak in the wavenumber spectrum enters the acoustic wavenumber range, leading to an increase in the sound power and radiation efficiency.

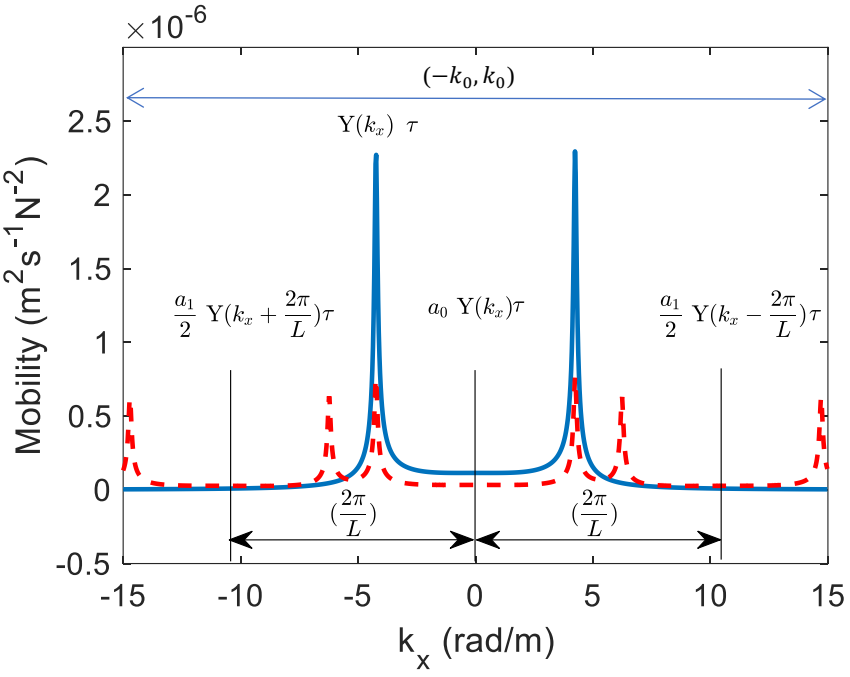

(a)

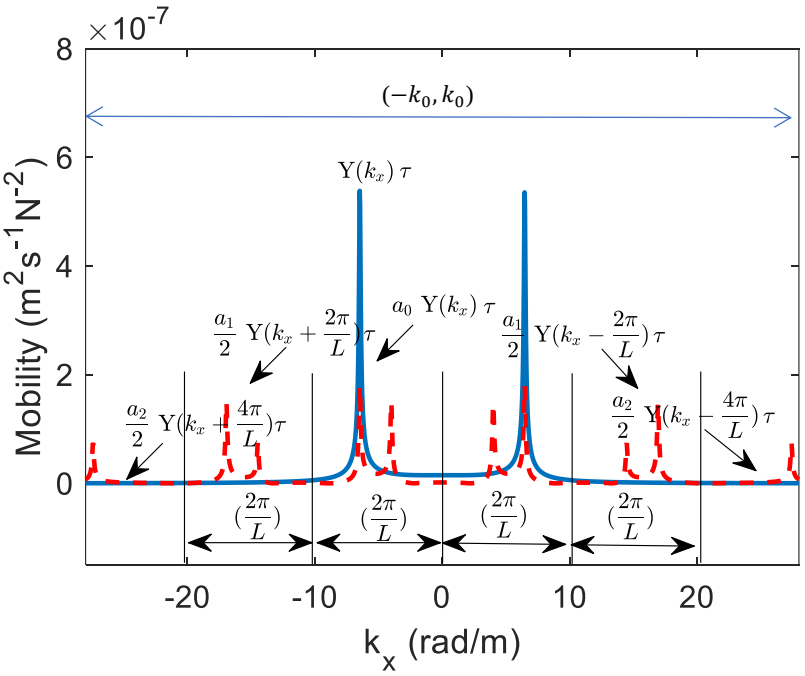

(b)

Figure 15. Comparison of mobility in the wavenumber domain, magnitude. (a) 810 Hz, (b) 1505 Hz. - - - : discrete sleepers with spacing L = 0.6 m, ——— : continuous sleepers.

According to the above analysis of wavenumber spectra, the components $\tilde{Y}\left(k_x + \frac{2n\pi}{L}\right)\frac{a_n}{2}$ and $\tilde{Y}(k_x)$ have the same spectrum but the first has been shifted in wavenumber and scaled by $a_n/2$. Moreover, assuming that waves with different wavenumbers can be treated as incoherent, their contributions to the sound power will depend on their relative squared amplitudes. Thus, their contributions to the power are scaled by a factor $(a_n/2)^2$. When a new wave becomes supersonic, an extra term $(a_n/2)^2$ is added to the ratio of sound power. In the case presented in Figure 14(b), the ratio of the sound power of the discrete sleepers to the continuous sleepers can be approximated by $[{a_0}^2 + (a_1/2)^2]$. When more waves contribute, the ratio of sound powers becomes approximately $[{a_0}^2 + \sum_{i=1}^{N}(a_i/2)^2]$.

To show the influence of the coefficients a_n, Figure 16(a) plots a_n against the index *n*. The coefficients a_n appear with either positive or negative signs, and a_n generally decreases in magnitude with increasing *n*. Some values are zero, such as a_3 for $L = 0.6$ m; these wavenumber branches will therefore not contribute to the response. To show the expected ratio of sound powers, the factor $[{a_0}^2 + \sum_{i=1}^{N}(a_i/2)^2]$ is plotted in decibels as a function of *N* in Figure 16(b). When *N* = 0, only the main lobe of the wavenumber spectrum contributes, and this factor is equal to $a_0^2 = (2a/L)^2$, as noted earlier. As additional waves contribute, the factor converges approximately to $2a/L$. The results in Figure 16(b) for small and large values of *N* agree well with the low and high frequency limits found in Figure 11(b), see also Table 2.

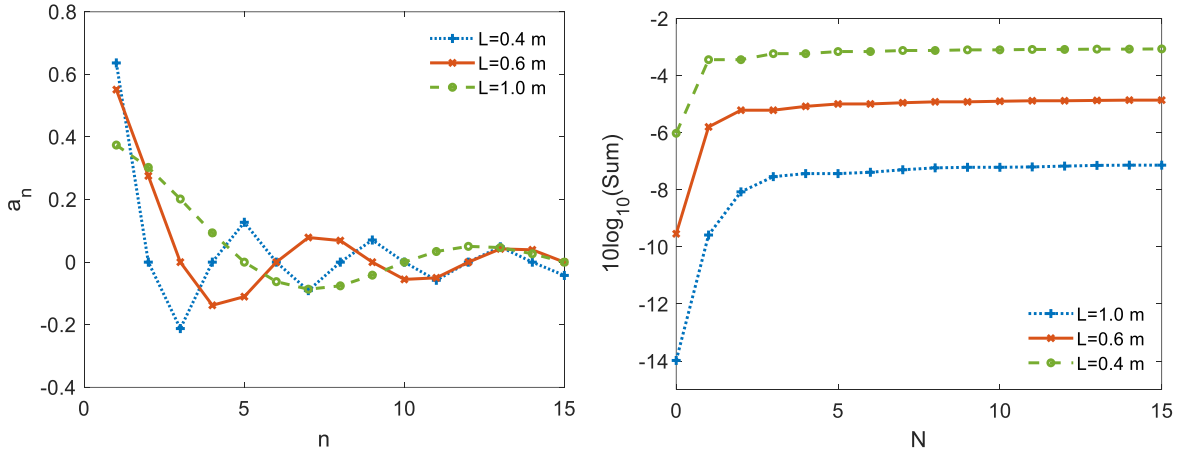

(a) (b)

Figure 16. (a) The coefficients a_n plotted against *n*, (b) $10\log_{10}[{a_0}^2 + \sum_{i=1}^{N}(a_i/2)^2]$ plotted against *N*.

6. Conclusions

A method is proposed to model the sound radiation from discretely spaced railway sleepers using a 2.5D method. A series of rectangular windows are used to create the velocity spectrum of the sleepers in the wavenumber domain. Results are compared with a Rayleigh integral approach, which confirms that the proposed method gives reliable predictions of the sound power and radiation efficiency of the discretely spaced sleepers.

The sleeper spacing is shown to have important influence on the sound radiation. The spectrum of response in the wavenumber domain contains multiple waves, shifted in wavenumber by multiples of $2\pi/L$, where L is the sleeper spacing, as found by Theyssen [25] and Sheng et al. [30]. At low frequency, only the fundamental wave corresponding to the rail wavenumber radiates power to the far field; the ratio of the sound power of discrete sleepers to that of continuous sleepers is equal to the square of the width-to-spacing ratio, $(2a/L)^2$. As the frequency increases, new wave branches enter the acoustic wavenumber range. At these frequencies, the sound power of the discrete sleepers suddenly increases and peaks appear in the radiation efficiency. At high frequency, where several waves radiate, the ratio of the sound powers shows small fluctuations but gradually converges to a constant value equal to the ratio of areas.

Declaration of Competing Interest

The authors declare that they have no known competing financial interests or personal relationships that could have appeared to influence the work reported in this paper. Data published in this paper are available at the University of Southampton repository at https://doi.org/10.5258/SOTON/D2644.

Credit authorship contribution statement

Hui Li: Conceptualization, Methodology, Software, Validation, Writing - original draft.
Xinbiao Xiao: Methodology, Validation.
David Thompson: Conceptualization, Methodology, Software, Writing - review & editing, Supervision.

Giacomo Squicciarini: Conceptualization, Supervision.

Acknowledgements

This work has been funded by the National Natural Science Foundation of China (No. U1934203), and the Sichuan Science and Technology Program (2020YJ0076).

References

[1] D. Thompson, Railway noise and vibration: mechanisms, modelling and means of control, Elsevier, 2008.

[2] P.J. Remington, Wheel/rail noise-Part IV: Rolling noise, Journal of Sound and Vibration 46(3) (1976) 419-436.

[3] P.J. Remington, Wheel/rail rolling noise, I: Theoretical analysis, Journal of the Acoustical Society of America 81 (1987) 1805-1823.

[4] D. Thompson, B. Hemsworth, N. Vincent, Experimental validation of the TWINS prediction program for rolling noise, part 1: description of the model and method, Journal of Sound and Vibration 193(1) (1996) 123-135.

[5] D. Thompson, P. Fodiman, H. Mahé, Experimental validation of the TWINS prediction program for rolling noise, part 2: results, Journal of Sound and Vibration 193(1) (1996) 137-147.

[6] D.J. Thompson, 1993, Wheel-rail noise generation, part II: wheel vibration. Journal of Sound and Vibration, 161(3), 401-419.

[7] D.J. Thompson, 1993, Wheel-rail noise generation, part III: rail vibration. Journal of Sound and Vibration, 161(3), 421-446.

[8] D.J. Thompson, C.J.C. Jones, 2002, Sound radiation from a vibrating railway wheel. Journal of Sound and Vibration, 253(2), 2002, 401 – 419.

[9] T. Zhong, G. Chen, X. Sheng, X. Zhan, L. Zhou, J. Kai. Vibration and sound radiation of a rotating train wheel subject to a vertical harmonic wheel–rail force. Journal of Modern Transportation 26(2) (2018), 81–95.

[10] F. Fabre, J. Theyssen, A. Pieringer and W. Kropp. Sound radiation from railway wheels including ground reflections: a half-space formulation for the Fourier boundary element method. Journal of Sound and Vibration 493 (2021) 115822.

[11] D.J. Thompson, C.J.C. Jones, N. Turner, 2003, Investigation into the validity of two-dimensional models for sound radiation from waves in rails. Journal of the Acoustical Society of America, 113(4, pt1), 2003, 1965-1974.

[12] X. Zhang, G. Squicciarini, D.J. Thompson, 2016, Sound radiation of a railway rail in close proximity to the ground. Journal of Sound and Vibration 326, 111-124.

[13] C.M. Nilsson, C.J.C. Jones, D.J. Thompson, J. Ryue, A waveguide finite element and boundary element approach to calculating the sound radiated by railway and tram rails, Journal of Sound and Vibration 321(3-5) (2009) 813-836.

[14] J. Ryue, S. Jang, D.J. Thompson, A wavenumber domain numerical analysis of rail noise including the surface impedance of the ground, Journal of Sound and Vibration 432 (2018) 173-191.

[15] W. Sun, D. Thompson, M. Toward, Z. Zeng, 2020, Modelling of vibration and noise behaviour of embedded tram tracks using a wavenumber domain method, Journal of Sound and Vibration 481 (2020) 115446.

[16] X. Sheng, G. Cheng, D. Thompson, 2020, Modelling wheel/rail rolling noise for a high-speed train running along an infinitely long periodic slab track. Journal of the Acoustical Society of America 148(1) 174-190.

[17] X. Zhang, H. Jeong, D.J. Thompson, G. Squicciarini, 2019, The noise radiated by ballasted and slab tracks. Applied Acoustics 151, 193-205.

[18] J. Theyssen, A. Pieringer, W. Kropp. The influence of track parameters on the sound radiation from slab tracks. Proceedings of the 13th International Workshop on Railway Noise, Ghent, Belgium, September 2019. Ed. G. Degrande et al. Notes on Numerical Fluid Mechanics and Multidisciplinary Design. Vol. 150. 2021, pp. 90–97.

[19] D. Duhamel, Efficient calculation of the three-dimensional sound pressure field around a noise barrier, Journal of Sound and Vibration 197(5) (1996) 547-571.

[20] X. Zhang, D. Thompson, E. Quaranta, G. Squicciarini, An engineering model for the prediction of the sound radiation from a railway track, Journal of Sound and Vibration 461 (2019) 114921.

[21] D.J. Thompson, M.H.A. Janssens, F.G. de Beer, TWINS: Track-Wheel Interaction Noise Software, theoretical manual (version 3.0), TNO report HAG-RPT-990211, Delft, 1999.

[22] J.C.O. Nielsen, Acoustic optimization of railway sleepers. Journal of Sound and Vibration 231 (2000) 753-764.

[23] X. Zhang, D.J. Thompson, G. Squicciarini, 2016, Sound radiation from railway sleepers, Journal of Sound and Vibration 369, 178-194.

[24] H. Li, D. Thompson, G. Squicciarini, X. Liu, M. Rissmann, F.D. Denia, J. Giner-Navarro, Using a 2.5 D boundary element model to predict the sound distribution on train external surfaces due to rolling noise, Journal of Sound and Vibration 486 (2020) 115599.

[25] J.S. Theyssen, Simulating rolling noise on ballasted and slab tracks: vibration, radiation, and pass-by signals. Doctoral thesis, Chalmers University of Technology, 2022.

[26] X. Zhang, D.J Thompson, Q. Li, D. Kostovasilis, M.G.R Toward, G. Squicciarini, J. Ryue, A model of a discretely supported railway track based on a 2.5D finite element approach. Journal of Sound and Vibration 438 (2019) 153-174.

[27] S.L. Grassie, Dynamic modelling of concrete railway sleepers, Journal of Sound and Vibration 187 (1995) 799-813.

[28] H. Kim, J. Ryue, D. J. Thompson, A. D. Müller, Application of a wavenumber domain numerical method to the prediction of the radiation efficiency and sound transmission of complex extruded panels, Journal of Sound and Vibration 449 (2019) 98-120

[29] F. Fahy, D. Thompson, Fundamentals of sound and vibration, second edition, CRC Press. 2016.

[30] X. Sheng, T. Zhong, Y. Li, Vibration and sound radiation of slab high-speed railway tracks subject to a moving harmonic load, Journal of Sound and Vibration, 395 (2017) 160-186.

[31] H.A. Schenck, Improved integral formulation for acoustic radiation problems, The Journal of the Acoustical Society of America 44(1) (1968) 41-58.

[32] J. W. Strutt (Lord Rayleigh), The theory of sound, Dover, 1945.

[33] D.J. Mead, Plates with regular stiffening in acoustic media: Vibration and radiation. The Journal of the Acoustical Society of America 88 (1990) 391-40.